This work appeared on 2014-12-16

Applied Physics Letters **105**, 244104 (2014)
doi: 10.1063/1.4904713
View online: http://dx.doi.org/10.1063/1.4904713 with free download until 2015-01-15

Localized heating of electrons in ionization zones: Going beyond the Penning-Thornton paradigm in magnetron sputtering

André Anders

Lawrence Berkeley National Laboratory, 1 Cyclotron Road, Berkeley, California 94720, USA

Electronic mail: aanders@lbl.gov

Acknowledgments

A. Rauch, M. Panjan, P. Ni, J. Andersson Y. Yang and J. Liu are gratefully acknowledged for their role in producing many images of ionization zones and discussing the underlying physics. Work at LBNL is supported by the U.S. Department of Energy, under Contract No. DE-AC02-05CH11231.

Abstract

The fundamental question of how energy is supplied to a magnetron discharge is commonly answered by the Penning-Thornton paradigm invoking secondary electrons. Huo *et al*. (Plasma Sources Sci. Technol. 22, 045005, (2013)) used a *global* discharge model to show that electron heating in the electric field of the magnetic presheath is dominant. In this contribution, this concept is applied *locally* taking into account the electric potential structure of ionization zones. Images of ionization zones can and should be interpreted as diagrams of the localization of electric potential and related electron energy, where certain collisions promote or dampen their formation.

Since the broad introduction of the sputtering magnetron for the deposition of thin films in the 1970s, a large number of papers were published elucidating the many aspects of the discharge in crossed electric and magnetic fields, particle fluxes, and applications. Among the early work, Thornton's description[1] captures our conventional understanding of the principles. We find the importance of classical concepts like the role of charged particle motion in crossed electric and magnetic fields, and the anticipation that collective effects (waves and instabilities) are important as they govern charged particle transport and thereby determine the discharge impedance and overall performance.

Publications in recent years have confirmed that discharge plasma is often structured,[2-4] which seems especially relevant when we consider high power impulse magnetron sputtering (HiPIMS), an emerging technology for energetic film deposition.[5] One of the fundamental questions we still wrestle with is how the magnetron discharge is "energized," i.e., how the energy supplied by the power supply is actually brought to the electrons that cause excitation and ionization and thereby enable the very functioning of the discharge. The conventional paradigm, as summarized by Thornton,[1] was originally described by Penning.[6] It postulates that plasma generation is based on the supply of energy via secondary electrons (SEs) from the target. SEs are critically important because they travel through the cathode sheath and pick up kinetic energy equivalent to the sheath voltage: $E_{SE} = eV_{sheath}$. The sheath accommodates most (about 80-90%) of the applied voltage; this is usually several 100 V. Using a simple energy conservation argument, each SE has the capability of producing multiple ion-electron pairs, namely up to eV_{sheath}/E_{ion}, where E_{ion} is the ionization energy. The ratio eV_{sheath}/E_{ion} ranges from about 20 ($E_{ion} \sim 12-24$ eV, for noble gas ions) to about 100 ($E_{ion} \sim 5-9$ eV, for HiPIMS conditions where metal ionization is important).

Penning[6] was well aware, in 1936, that this mechanism has some difficulties when the glow discharge is in a magnetic field, namely that the number of available secondary electrons is very small because (a) the SE yield γ_{SE} from primary ion impact is small to begin with (typically 0.1 or less), and (b) most SEs would be re-captured when the magnetic field vector is approximately parallel to the target surface. The latter point can be seen when considering the equation of motion (neglecting all kinds of collisions)

$$\frac{d\mathbf{v}}{dt} = \frac{e}{m_e}\left(\mathbf{E} + \mathbf{v} \times \mathbf{B}\right) \tag{1}$$

where the second term of the right hand side, the Lorentz force, causes electrons to gyrate around magnetic field lines. A SE is therefore likely to return to the cathode surface and be re-captured after completing about ½ of one gyration.

The electron gyration "radius" is given by

$$r_{g,e} = \frac{m_e u_{e\perp}}{eB} = \frac{u_{e\perp}}{\omega_e}. \tag{2}$$

where m_e is the electron mass, $u_\perp$ is the electron's velocity component perpendicular to the magnetic field $\mathbf{B}$, and $B = |\mathbf{B}|$. In Eq. (2) the gyration frequency $\omega_e = eB/m_e$ was used. When the electron transverses a region with an electric field, the velocity $u_\perp$ is not constant due to the first term of the r.h.s. of Eq. (1), an effect that causes the well-known $\mathbf{E} \times \mathbf{B}$ drift for those electrons that can complete gyration. Penning[6] suggested that while the yield γ_{SE} is reduced by recapture it could still be sufficiently high for three reasons: (i) surface roughness of the cathode, (ii) the magnetic field vector has in most locations a tilt relative to the target surface, and (iii) the SE collides with other particles while completing its first half-gyration. Buyle and coworkers[7] analyzed the situation and they came to the conclusions that the recapture probability p_{recap} is determined by the mean free path of the SE and the average distance travelled before recapture occurs. Since the tilt angle ϑ of the magnetic field relative to the target surface depends on location, the recapture probability $p_{recap}(\vartheta)$ depends on the location of electron emission. Costin and coworkers[8] derived an expression for the net SE emission yield, an effective yield useful to energize the discharge, as follows:

$$\gamma_{net} = \left(1 - p_{recap}\right)\gamma_{SE} = \left(1 - \frac{\omega_e^2 \cos^2 \vartheta}{\nu_e^2 + \omega_e^2}\right)\gamma_{SE} \tag{3}$$

which accounts for recapture, its angle dependence, and the density of neutrals as ν_e is the total momentum transfer frequency for electron–neutral collisions.

It has been known for some years that the issue of very low γ_{net} could be further aggravated when singly charged metal ions replace the noble gas ions during each HiPIMS pulse.[9] The yield for singly charged metal ions is zero based on Baragiola's empirical yield formula[10] for clean targets

$$\gamma_{SE} = \begin{cases} 0.032\left(0.78\,E_{pot} - 2\phi\right) & \text{for } 0.78\,E_{pot} > 2\phi \\ 0 & \text{else} \end{cases}, \tag{4}$$

where E_{pot} is the potential energy of the impacting ion (that is, its ionization energy, e.g. 6.82 eV for Ti^{+}), and ϕ is the work function (e.g. 4.3 eV for Ti). It was therefore proposed[9,11] that the generation of doubly and higher charged ions must be critical to HiPIMS operation.

An new mechanism, recently presented by Huo *et al*.,[12] greatly reduces or even eliminates the need for secondary electrons. Using a *global* model of the magnetron discharge, Huo *et al.*[12] showed that the voltage drop in the magnetic presheath can lead to very significant energy dissipation and electron heating. Even as the voltage drop in the magnetic presheath (a.k.a. ionization region between sheath and bulk plasma) is much smaller than the voltage drop in the sheath, the number of electrons experiencing the voltage drop in the presheath is orders of magnitude greater, and hence electron heating in the presheath outweighs energizing according to the Penning-Thornton paradigm. Electrons energized in the presheath will on average gain energy corresponding to ½ of the voltage drop in the presheath (electrons carry about ½ of the current while positive ions, moving to target, carry the rest of the discharge current[12]); the actual fraction of current-carrying particles and energy gain depends on location and the local potential structure, as will be argued). Measurements of the electron distribution function at some distance from the target revealed thermal and "energetic" electrons, the latter being distinct from the thermal but with an energy of less than 15 eV.[13,14]

It is known that a relatively large potential drop can exist in quasineutral plasma when a magnetic field is present because electron motion perpendicular to the magnetic field is impeded. The electric field is perpendicular to the magnetic field lines. To enable operation of the discharge at low gas pressure (~1 Pa), electrons are confined, e.g., by a closed-drift configuration in a magnetron. The magnetic field arches over the target and the magnetic presheath is most expanded where the **B**-field is approximately parallel to the target (Fig. 1). This is the region of most ionizing collisions caused by electrons. Positive ions created here are accelerated to the negatively biased target, causing sputtering and the formation of the well-known erosion racetrack. A large potential drop in the plasma has been linked with the Hall parameter $h = \omega_{ce}/\nu_e$, where ω_{ce} is the electron cyclotron angular frequency and ν_e is the electron collision frequency.[15] With increasing distance from the target, the magnetic field weakens, the Hall parameter decreases, and less of a voltage drop is accommodated.

It is well known that electrons in the magnetic presheath in the region above the racetrack gyrate around the arched field lines and "bounce" back-and-forth as the magnetic field lines converge toward the target and intersect the presheath-sheath boundary. A gyrating electron periodically reverses direction due to the magnetic mirror effect, as indicated by Thornton[1] in his

Fig. 2f, or due to the electric field when reaching the sheath boundary. Averaging over gyration and back-and-forth motion leads to the electron $\mathbf{E}\times\mathbf{B}$ drift (and other drifts such as the $\nabla B\times\mathbf{B}$ drift). Electrons gain energy as they diffuse to magnetic field lines where the potential is higher.[12] In this contribution, the idea of presheath heating of electrons[12] is examined on a *local* level, and it is shown that there is a interdependence between presheath heating of electrons, the formation (and disappearance) of ionization zones[2-4] (a.k.a. spokes[11,16,17]), and associated potential humps.[18]

Fast imaging of HiPIMS[2-4,11,19] and direct current magnetron sputtering[20] (dcMS) plasmas indicated that ionization rate and emission of light and particles are usually not uniformly distributed but concentrated in bright zones that move along the racetrack. Additionally, measurements of charged particle fluxes have revealed important features: (a) ion and electron fluxes appear in short pulses (jets),[21] (b) doubly charged ions have approximately twice the energy of singly charged ions,[18,21] and (c) ions emitted in the $\mathbf{E}\times\mathbf{B}$ direction have several 10 eV higher energy than ions going in the opposite direction, i.e., leaving the magnetron in the $-\mathbf{E}\times\mathbf{B}$ direction.[18] All of these features can be explained[18] assuming that an ionization zone is a locations of a potential hump of several 10 V. Consistent with Maxwell's equations, each potential hump is surrounded by an electric double layer.[16,18]

The electric potential distribution in the presheath and especially around the ionization zones is difficult to determine in a direct manner as probe measurements very close to the target excessively disturb the discharge. Fortunately, plasma potential data are available[22-24] measured at some distance from the target. They can be extrapolated to the relevant region up to the presheath-sheath boundary (Fig. 1). The data suggest that a drop of the order 100 V occurs from the sheath edge (at about z = 0.5 mm from the target surface) to the plasma outside the magnetic presheath (at about z = 25 mm; those distance values may vary depending on the specifics of the magnetron and discharge parameters).

The most detailed data[23] were obtained by averaging over 100 times for each location, i.e. they cannot give information on the electric potential structure for an individual, moving ionization zone. Time-averaged, the potential distribution in a plane perpendicular to the direction of the racetrack, ξ , looks like a funnel (*cf*. Fig. 7 of ref.[23], and Fig. 1 here). The derivative $\mathbf{E}=-\nabla V$ gives an electric field that accelerates ions and gives rise to the $\mathbf{E}\times\mathbf{B}$ drift of electrons. As shown in Fig. 1, the arched magnetic field lines are intersecting the electric field approximately perpendicularly, making the magnetic field lines approximate equipotential lines.

The situation is different when an ionization zone is present: the local electric field is significantly changed by the space charge of the double layer while the magnetic field is only slightly altered by the currents in the plasma. Consider drifting electrons encountering the double layer of an ionization zone as electron drift velocity is much greater than the drift velocity of ionization zones.[3,4] According to the local electric field, with the higher electric potential located in the hump, the electron drift is re-directed *towards* the target as shown in Fig. 2 (a).

In a first approximation, electrons drift in a surface of equal potential because $\mathbf{E}\times\mathbf{B}$ is by definition perpendicular to the fields. Without interactions, electrons would drift "under" the hump to emerge on the other side and continue drifting along the racetrack. However, as the ionization zone is a region of enhanced plasma density, electrons experience an enhanced rate of collisions with neutrals, ions, and electrons. Collisions with neutrals could lead to ionization provided electron energy exceeds the ionization energy, or to cross-field diffusion. Electrons moving toward the potential hump center gain energy. Conversely, electrons moving away from the hump can lose energy as this a region of lower potential. The effect of electron-electron interaction can be expressed by the gradient of the electron pressure, $\nabla p_e = \nabla\left(n_e k T_e\right)$, which is directed away from the potential hump.

Electrons upstream of the hump have no gain mechanism but are less energetic than average as they are re-directed closer to the target and a fraction is pushed to lower potential. This appears to be consistent with the observation that less light is emitted upstream of the potential hump, sometimes labeled as a "cut" of emission before the hump (Fig. 3). The light emission "cut" is visible in a direction perpendicular to the racetrack (i.e. the radial direction) because the gyration motion of electrons is approximately along the magnetic field lines.

Electrons in the thin but dense region between the target and potential hump are subject to cross-**B**-field transport facilitated by collisions as well as micro-instabilities (collective effects).[25] Either way, electrons moving to the potential hump (dotted lines with arrows in Fig. 2(a)) can be energized beyond the ionization energy as the potential drop in the presheath is several 10 V. Figure 2 illustrates the potential structure in the azimuthal, radial and axial directions, considering the changes when the ionization zone is present.

Up to now, the potential hump in an ionization zone was *a priori* assumed. One needs to justify this assumption by showing that the proposed mechanism would sustain the potential hump. The electron drift velocity is faster than the zone velocity, however, one needs to show that electrons can actually escape from the hump, leaving positive ions behind, and thereby enabling the formation of a double layer that defines the hump. Electrons can only escape if their energy is greater than the smallest potential difference between the hump and its surroundings:

$$E_e > \min\left[e\left(V_{hump} - V_{sur}\right)\right] \tag{5}$$

where, according to the localized energizing model, the electrons can gain energy from the sheath edge to the peak of the hump:

$$E_e = e\left(V_{hump} - V_{edge}\right), \tag{6}$$

which can reach several 10 V and thus readily exceeding the ionization energies of the neutrals present. Electrons sufficiently energized can make inelastic collisions: now it is not trivial if the remaining energy is large enough for escape. Using (5) and (6) one can write the condition for escape as

$$e\left(V_{hump}-V_{edge}\right)-\sum_{\alpha}E_{e\alpha}>\min\left[e\left(V_{hump}-V_{sur}\right)\right] \tag{7}$$

where $\sum_{\alpha}E_{e\alpha}$ is the cumulative loss of energy through collisions with particles of type α. To evaluate this situation one needs to consider detailed rate equations and energy balance. It is clear that the energy gain (6) needs to be at least the ionization energy of the prevalent neutral in order to produce at least one ion via this localized mechanism of electron heating. Under certain conditions, most prominently when there are many neutrals, e.g. when a high gas pressure is used, electrons are cooled by collisions with the gas. In this case, condition (7) may be violated. Electrons are then trapped by the potential hump, which makes the hump shallower or disappear. Disappearance of ionization zones has indeed be observed, namely when the discharge power is high.[26] Our observations also indicated a disappearance or "smoothing" of ionization zones at high pressure, or more precisely, at high neutral atom density, which can be achieved even in the pure self-sputtering mode in vacuum.[27]

Spectroscopic imaging of ionization zones[19] revealed that the higher the excitation level, the sharper and more spatially limited the visible emission are, which can be interpreted as the shape of the potential hump (Fig. 3). This suggests that spectrally integrated[2-4,11] and spectrally selected[19] images show not just regions of enhanced excitation and ionization but regions of elevated electric potential. Images of ionization zones can and should be interpreted as distributions of electric potential and related electron energy. Electrons reaching the center of the ionization zone at greater distances from the target are most energetic as judged by the upper excitation level of the emitted spectral lines, which is consistent with images — this time seen from the side. Local energizing of electrons in the magnetic presheath, the appearance of ionization zones, the low-light "cut", and the formation of potential humps are related. Secondary electrons of the Penning-Thornton paradigm are merely supplemental, as it is sufficient to follow the "energy fate" of drifting electrons to obtain the processes and images described above.

As a side note, one can see that the proposed potential structure has the highest surface electric field at the edges of the racetrack (Fig. 2, bottom), which may explain observations[28,29] that arcing preferentially occurs at the edges of the racetrack rather than inside.

In conclusion, taking the hypothesis that each ionization zone is associated with a potential hump enclosed by an electric double layer, one finds that drifting electrons are deflected toward the target when they arrive at an ionization zone. Once close to the target and in the relatively dense plasma of the ionization zone, they are energized via the potential difference as they reach greater heights above the target through collisions and microinstabilities. Energizing electrons in the ionization zone enables a feedback mechanism for maintaining and amplifying the ionization zone, namely the potential hump results from the inertia of ions that are left behind as a fraction of electrons escapes from the ionization zone. Since inelastic collisions of energized electrons are the cause for the light emitted from the ionization zones, such zones are closely related to the local electron energy. This suggests interpreting images of ionization zones as images of plasma potential and electron energy.

References

1 J. A. Thornton, J. Vac. Sci. Technol. **15,** 171 (1978).

2 A. Kozyrev, N. Sochugov, K. Oskomov, A. Zakharov, and A. Odivanova, Plasma Physics Reports **37,** 621 (2011).

3 A. P. Ehiasarian, A. Hecimovic, T. de los Arcos, R. New, V. Schulz-von der Gathen, M. Böke, and J. Winter, Appl. Phys. Lett. **100,** 114101 (2012).

4 A. Anders, P. Ni, and A. Rauch, J. Appl. Phys. **111,** 053304 (2012).

5 U. Helmersson, M. Lattemann, J. Bohlmark, A. P. Ehiasarian, and J. T. Gudmundsson, Thin Solid Films **513,** 1 (2006).

6 F. M. Penning, Physica **3,** 873 (1936).

7 G. Buyle, W. De Bosscher, D. Depla, K. Eufinger, J. Haemers, and R. De Gryse, Vacuum **70,** 29 (2003).

8 C. Costin, G. Popa, and G. Gousset, J. Optoelectron. Adv. Mater. **7,** 2465 (2005).

9 A. Anders, Appl. Phys. Lett. **92,** 201501 (2008).

10 R. A. Baragiola, E. V. Alonso, J. Ferron, and A. Oliva-Florio, Surf. Sci. **90,** 240 (1979).

11 A. Hecimovic, M. Böke, and J. Winter, J. Phys. D: Appl. Phys. **47,** 102003 (2014).

12 C. Huo, D. Lundin, M. A. Raadu, A. Anders, J. T. Gudmundsson, and N. Brenning, Plasma Sources Sci. Technol. **22,** 045005 (2013).

13 J. T. Gudmundsson, J. Alami, and U. Helmersson, Appl. Phys. Lett. **78,** 3427 (2001).

14 A. Vetushka and A. P. Ehiasarian, J. Phys. D: Appl. Phys. **41,** 015204 (2008).

15 J.-P. Boeuf and B. Chaudhury, Phys. Rev. Lett. **111,** 155005 (2013).

16 N. Brenning, D. Lundin, T. Minea, C. Costin, and C. Vitelaru, J. Phys. D: Appl. Phys. **46,** 084005 (2013).

17 S. Gallian, W. N. G. Hitchon, D. Eremin, T. Mussenbrock, and R. P. Brinkmann, Plasma Sources Sci. Technol. **22,** 055012 (2013).

18 A. Anders, M. Panjan, R. Franz, J. Andersson, and P. Ni, Appl. Phys. Lett. **103,** 144103 (2013).

19 J. Andersson, P. Ni, and A. Anders, Appl. Phys. Lett. **103,** 054104 (2013).

20 A. Anders, P. Ni, and J. Andersson, IEEE Trans. Plasma Sci. **42,** online 10.1109/TPS.2014.2334601 (2014).

21 M. Panjan, R. Franz, and A. Anders, Plasma Sources Sci. Technol. **23,** 025007 (2014).

[22] J. W. Bradley, S. Thompson, and Y. A. Gonzalvo, Plasma Sources Sci. Technol. **10,** 490 (2001).
[23] A. Rauch, R. Mendelsberg, J. M. Sanders, and A. Anders, J. Appl. Phys. **111,** 083302 (2012).
[24] A. Mishra, P. J. Kelly, and J. W. Bradley, J. Phys. D: Appl. Phys. **44,** 425201 (2011).
[25] F. F. Chen, *Plasma Physics and Controlled Fusion* (Plenum Press, New York, 1984).
[26] T. de los Arcos, V. Layes, Y. A. Gonzalvo, V. Schulz-von der Gathen, A. Hecimovic, and J. Winter, Journal of Physics D: Applied Physics **46,** 335201 (2013).
[27] J. Andersson, P. Ni, and A. Anders, IEEE Trans. Plasma Sci. **42,** online 10.1109/TPS.2014.2334600 (2014).
[28] F. G. Tomasel, D. Carter, H. Walde, J. J. Gonzalez, and G. McDonough, Plasma Sources Sci. Technol. **12,** 139 (2003).
[29] M. Lattemann, B. Abendroth, A. Moafi, D. G. McCulloch, and D. R. McKenzie, Diamond Rel. Mater. **20,** 68 (2011).

Figure Captions

Fig. 1 Composite image showing magnetic field (left) and electric field (right) of a 3" magnetron; $r = 0$ represents the center of the target. While the magnetic field, produced by permanent magnets and measured with a movable Hall probe, is almost independent of the discharge, the electric field varies with discharge conditions. The **E**-field distribution shown here was measured with an emissive probe, where the value at each location was obtained by averaging over 100 HiPIMS pulses; for more details see ref.[23]

Fig. 2 Schematic presentation of the proposed potential distribution, where ξ is the coordinate along the racetrack, r is the radial coordinate perpendicular to the racetrack, and z is the distance from the target surface. $\mathbf{E} \times \mathbf{B}$ drift of electrons is indicated by arrows; electrons entering the hump are energized (dashed arrows).

Fig. 3 Fast camera images of ionization zones in the emitted light of Al neutrals (left column) and Al ions (right column) in side-on and end-on view (upper and lower row, respectively). The regions of an electric double layer and high potential are indicated. Since the fast camera can only take one image at a time, the images shown are from different HiPIMS pulses. However, from the large number of images those were selected that represent similar conditions. For experimental details see ref.[19]

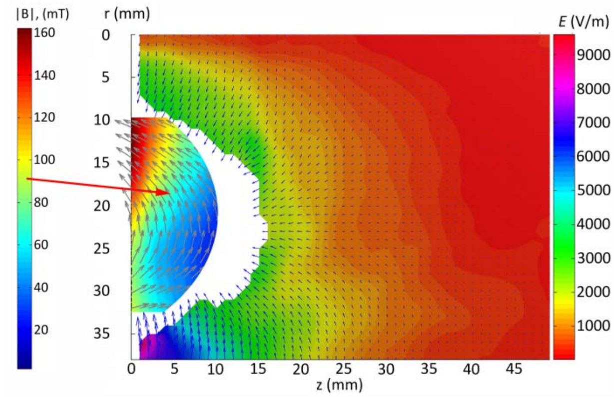

|B|, (mT)
160
140
120
100
80
60
40
20
r (mm)
0
5
10
15
20
25
30
35
E (V/m)
9000
8000
7000
6000
5000
4000
3000
2000
1000
0
5
10
15
20
25
30
35
40
45
z (mm)

Fig. 1

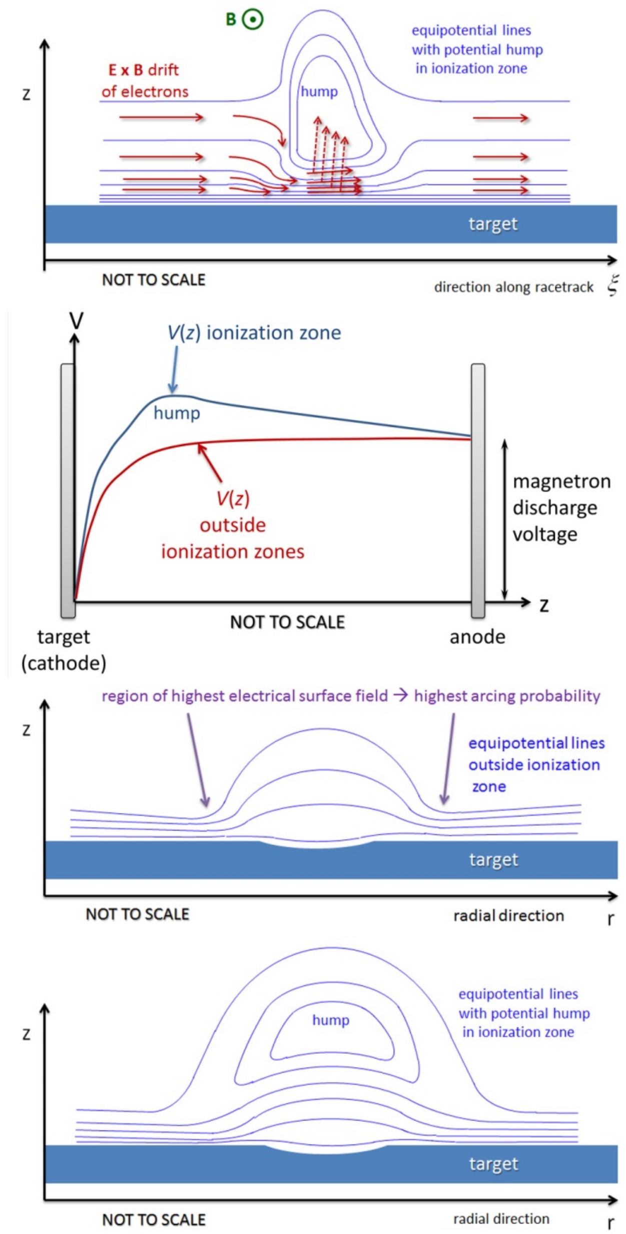
B
E x B drift
of electrons
z
hump
equipotential lines
with potential hump
in ionization zone
target
NOT TO SCALE
direction along racetrack ξ
V
$V(z)$ ionization zone
hump
$V(z)$
outside
ionization zones
magnetron
discharge
voltage
z
target
(cathode)
NOT TO SCALE
anode
region of highest electrical surface field → highest arcing probability
z
equipotential lines
outside ionization
zone
target
NOT TO SCALE
radial direction
r
z
hump
equipotential lines
with potential hump
in ionization zone
target
NOT TO SCALE
radial direction
r

Fig. 2

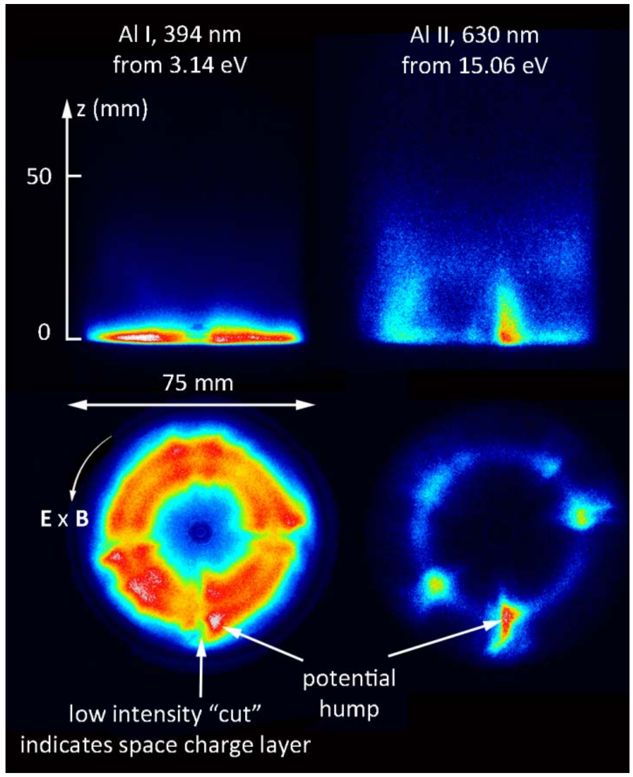
Al I, 394 nm
from 3.14 eV
Al II, 630 nm
from 15.06 eV
z (mm)
50
0
75 mm
E x B
potential
hump
low intensity "cut"
indicates space charge layer

Fig. 3